

## ***Chapter 3***

### ***Microbial characteristics and their association with sediment geochemical properties in 17 m deep estuarine core at Chokari, Mahi River Basin***

“The willpower is an intellectual courage to sustain determination.”

- Pandurang Shastri Athavale

### **3.1 Introduction**

Estuarine ecosystems are considered the most productive ecosystems in the world and have a vital role in maintaining global biogeochemical cycles (Chapman and Wang 2001; Maher and Eyre 2012; Jickells et al. 2016). Additionally, landscapes of estuarine terraces are widely used for various man-made activities such as agriculture and freshwater abstraction. Therefore, assessing estuarine ecosystem health is a major concern (Long and MacDonald 1998). Estuarine ecosystems comprise heterogeneous lithofacies ranging from tidal to fluvial sediments depending on temporal sea-level changes, hydrodynamics, and morphology of the estuary (Gingras et al. 2012). This results in a highly variable vertical stratification of sediments with different physicochemical parameters such as textural and geochemical characteristics.

Sediment physicochemical parameters have a pronounced influence on microbial parameters (Wilms et al. 2006; Thomas et al. 2015; Delgado-Baquerizo et al. 2017; Subrahmanyam et al. 2021). Further, microbial activities and diversity contribute to biogeochemical cycling, ecosystem functioning and stability (Gadd 2010; Bianchi 2007). Therefore, understanding the key environmental parameters that affect microbial parameters, can have implications for improving sediment quality or its health (Doran and Zeiss 2000). Several studies on microbial parameters of estuarine ecosystems and their interconnection with sediment physicochemical properties are focused on present-day (recently deposited) estuarine sediments, tidal/coastal freshwater wetlands, or relatively shallow sediments located at estuary (Mosier and Francis 2010; Hu et al. 2014; Zhou et al. 2017; Lv et al. 2016; Hong et al. 2019). Despite their ecological and economic importance, microbial parameters and their interconnection with sediment physicochemical properties are poorly understood in estuarine terraces (i.e., older sediment deposits observed at river estuaries).

In this study, our aims were (i) elucidation of microbial and physicochemical parameters within estuarine terrace (ii) identification of key environmental parameters that correlate with microbial parameters in estuarine terrace sediment deposits. To address these objectives we raised a 17 m deep core near Chokari on the left bank of the Mahi River estuary (Gujarat, Western India) at which Late Holocene estuarine sediments form 5-7 m cliffs on the pre-existing Late Pleistocene 15-20 m fluvial vertical cliffs (Maurya et al. 1997, 2000; Kusumgar et al. 1998; Raj et al. 1998). Samples from the core were subjected to analysis of microbial

parameters such as enzyme activities involved in C, N, P, and S cycling, microbial abundance and microbial diversity profiling by culture dependent and culture independent methods, as well as for analysis of physicochemical parameters such as texture, pH, salinity, organic C content, several major oxides, and trace elements. Key environmental parameters that correlate with microbial parameters have been determined by Pearson correlation analysis.

## **3.2 Results**

### **3.2.1 Stratigraphic sequences observed within Chokari (CRD) core**

As shown in Fig. 3.1, Chokari (CRD) core is located on the estuarine terrace of the Mahi River which is ~5 m above the present day high tide level. Core depth with respect to mean sea level is also indicated in Fig. 3.1. Representative photographs of split core liner showing the lithology of sediments present within CRD core are depicted in Fig. A-II (Appendix). The estuarine sediment deposits observed in the CRD core starts with a gravel layer (observed at ~7.7 m depth) overlain by sediments typically deposited in the estuarine environment that is characterized by the alternating influence of tidal fluctuation and freshwater influx. Relatively thinner bedding and rapid change in sediment composition conform to their deposition in an estuarine setting. In general, the estuarine sequence comprises several layers of tidal muds (clay), silty sand, sandy silt, and fine sand (Fig. 3.2). Further, estuarine sediments comprise organic matter rich clays to finely laminated silty clays and occasional horizontal stratification of the sandy and silty sediment layers (Fig. 3.2). Below gravel layer, the lithological horizons observed included silty sand, fine to medium sand, gravel and five distinct paleosol horizons with the presence of calcrete nodules suggests deposition in a fluvial environment with phases of no-deposition during which soil formation took place. (Fig. 3.2). The abundance of calcium carbonate nodules in the paleosols indicates the pedogenic transformation of fluvial sediments to the soil under semiarid climatic conditions (Fig. 3.2). It could be discerned that the top 7.7 m CRD core show estuarine sediment deposits (include Phase-II and Phase-1 estuarine deposits) and from ~7.7 to 17 m depth core show fluvial sediment deposits (Fig. 3.1, 3.2). Upper part of the core (up to ~5.5 m; Phase-II estuarine deposits) comprise [Late Holocene; Maurya et al. (1997b, 2000)] relatively finer grain particles (mainly enriched in silt content) as compared to the lower part (from ~5.5 to 17 m) of the core that comprises Phase-I estuarine [Late Holocene;

Maurya et al. (1997b, 2000)] and fluvial sediment deposits [Late Pleistocene; Maurya et al. (1997b, 2000)] (Fig. 3.2).

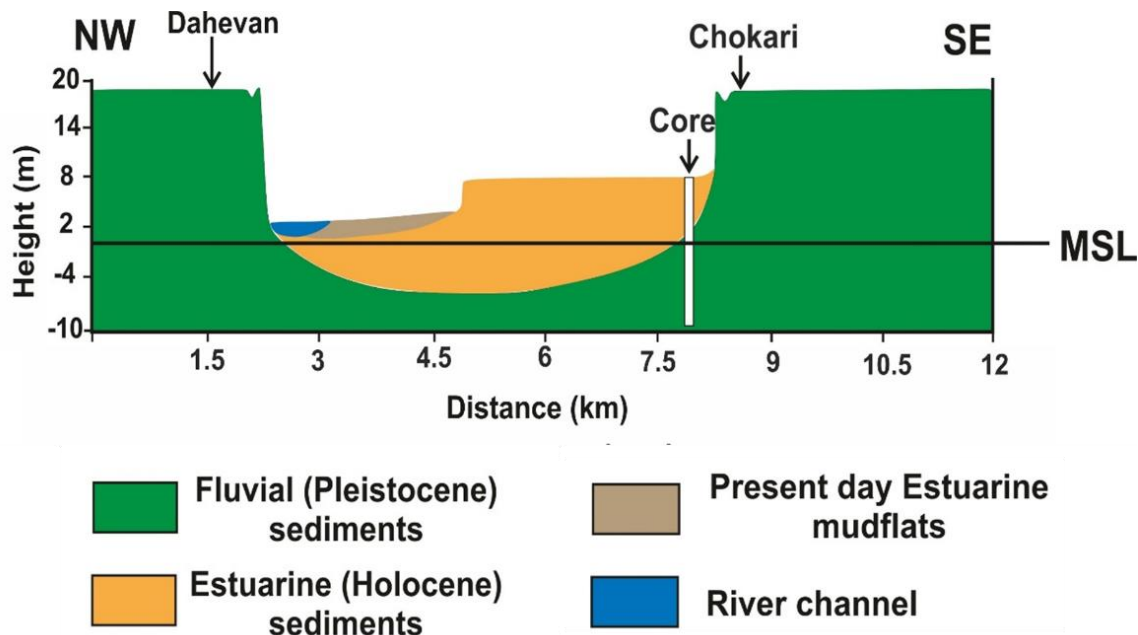


**Figure 3.1: Cross-section of CRD core drilling site.** The distance of the core drilling site from the river channel, core depth from the ground surface with respect to mean sea level (MSL) are indicated.

### 3.2.2 Physicochemical properties of CRD core samples

Obtained CRD core samples comprise total org. C content within a range of 1-5%,  $\text{Fe}_2\text{O}_3$  content within a range of 2-8%, MgO content within a range of 1-4%, and  $\text{P}_2\text{O}_5$  content within a range of 0.05-0.14%. CRD core samples have Cu content within a range of 20-213 ppm and Zn content within a range of 31-169 ppm. The salinity of CRD core samples was observed within the range of 0.2-1 ppt and the pH of sediment samples was observed within the range of 9-12. All physicochemical variables (except sand content) exhibited a significant negative correlation with depth ( $p < 0.05$ ). Additionally, salinity, pH, Org. C,  $\text{Fe}_2\text{O}_3$ , MgO,  $\text{P}_2\text{O}_3$ , Cu, and Zn content were significantly higher in the upper part (up to 5.5 m depth) of a core comprising phase-II estuarine sediment deposits as compared to the lower region (from 5.5 to 17 m depth) of a core comprising phase-I estuarine and fluvial sediment deposits (Welch's t-test,  $p < 0.05$ ).

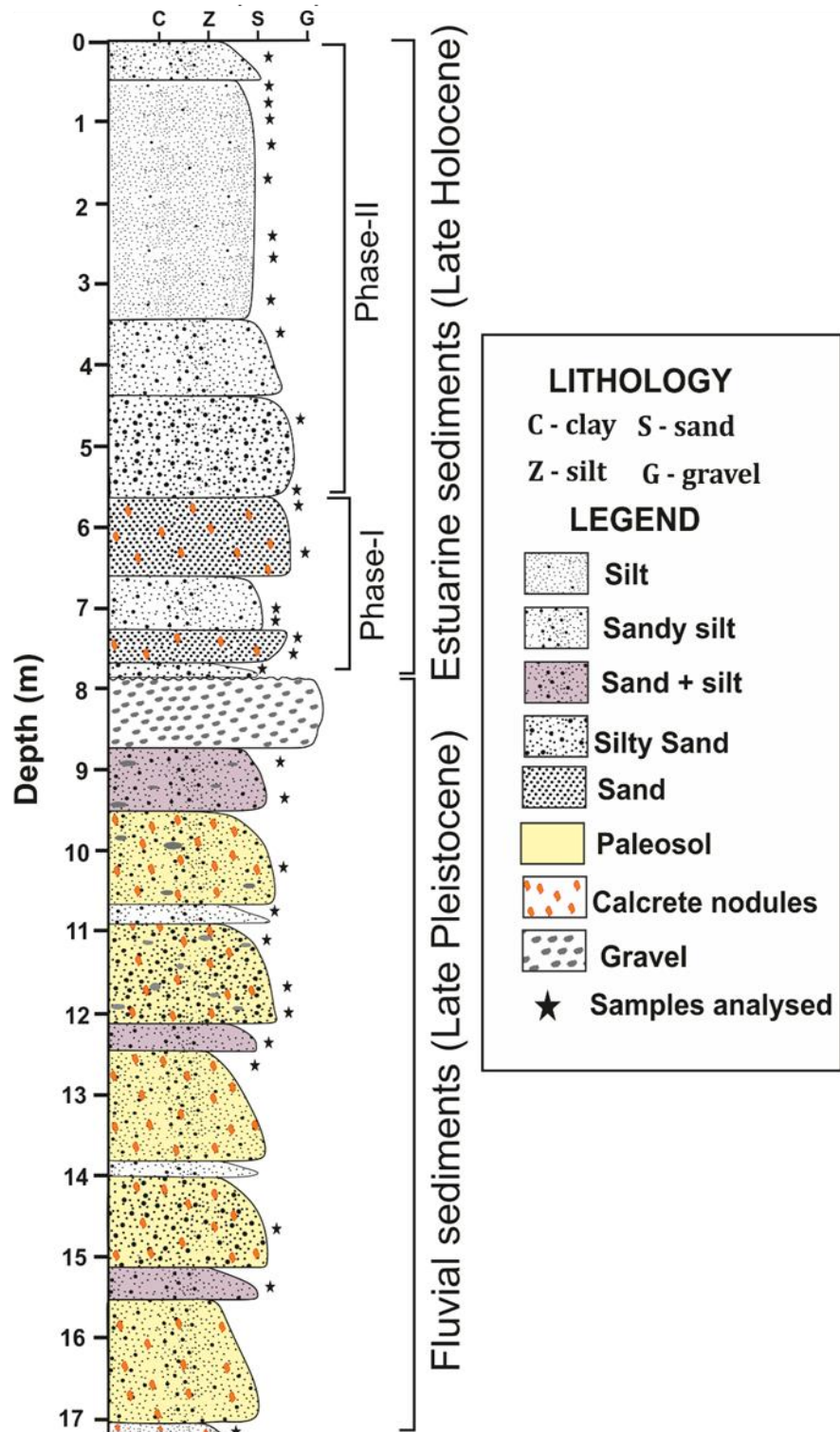


Figure 3.2: Litholog of Chokari (CRD) sediment core showing stratigraphic sequences (lithofacies) together with depositional phases. Stars denote the depth and stratigraphic sequence from which samples were analyzed.

### 3.3.3 Microbial enzyme activities and enzymatic stoichiometry within CRD core

Dehydrogenase activity (DHA) was high ( $27.8 \mu\text{g TPF g}^{-1}$  dry wt core sediment  $24\text{h}^{-1}$ ) in the top 0.25 m of the core and steeply decreased up to 5.5 m depth ( $3.87 \mu\text{g TPF g}^{-1}$  dry wt core sediment  $24\text{h}^{-1}$ ) (Fig. 3.3).  $\beta$ -glucosidase activity ( $\beta$ -GA), DHA, alkaline phosphatase activity (alkaline PA), protease enzyme (PTA), and arylsulfatase activity (ASA) were significantly high in the upper part (Phase-II estuarine deposits; up to depth  $\sim 5.5$  m) of CRD core as compared to the lower part (Phase-I estuarine and fluvial deposits; from  $\sim 5.5$  to 17 m) of CRD core (Fig. 3.3). Fluorescein diacetate hydrolysis activity (FDA HA) did not show a significant difference between the upper and lower part of the core although the highest activity (i.e.  $226.5 \mu\text{g fluorescein g}^{-1}$  dry wt core sediment  $4\text{h}^{-1}$ ) was observed in the top 0.25 m core. Alkaline phosphatase activity was observed within the range of 10.3 to  $154.2 \mu\text{g pNP g}^{-1}$  dry wt core sediment  $2\text{h}^{-1}$  with an average  $55.2 \mu\text{g pNP g}^{-1}$  dry wt core sediment  $2\text{h}^{-1}$ . On the whole, significantly high enzyme activities (except FDA HA) were observed in the upper part of the CRD core as compared to the lower part of the CRD core (Fig. 3.3).  $\beta$ -GA/Alkaline PA ratio observed within the range of 0.01 to 0.36 in the CRD core. Further, CRD core samples have less than 1 (except three samples) PTA/Alkaline PA ratio (Fig. 3.4). Both of these ratios indicate P limitation within the CRD core. Vector length (L) observed within the range of 0.013 to 1.19 suggesting lower C acquisition and the majority of samples (except three samples) exhibited vector angle  $>45^\circ$  suggesting P limitation. The scatter plot of ecoenzymatic stoichiometry also indicates P limitation (Fig. 3.4). Overall, ecoenzymatic stoichiometry analysis revealed P acquisition throughout 17 m CRD core.

### 3.3.4 Culturable bacterial counts and microbial gene abundance within CRD core

Plate counts on R2A agar indicate the presence of heterotrophic bacteria ranging from  $1.5 \times 10^5$  to  $2.1 \times 10^7$  (per gram dry weight of sediment) throughout the CRD core (Fig. 3.5). Bacterial 16S rRNA gene copy numbers were detected ranging from  $5.56 \times 10^6$  to  $7.5 \times 10^9$  per gram dry weight of sediment (Fig. 3.5). Denitrification is a major process that occurs in subsurface sedimentary environments under both anaerobic and aerobic conditions (Francis et al., 1989; Rice and Rogers, 1993; Chen and Strous, 2013).

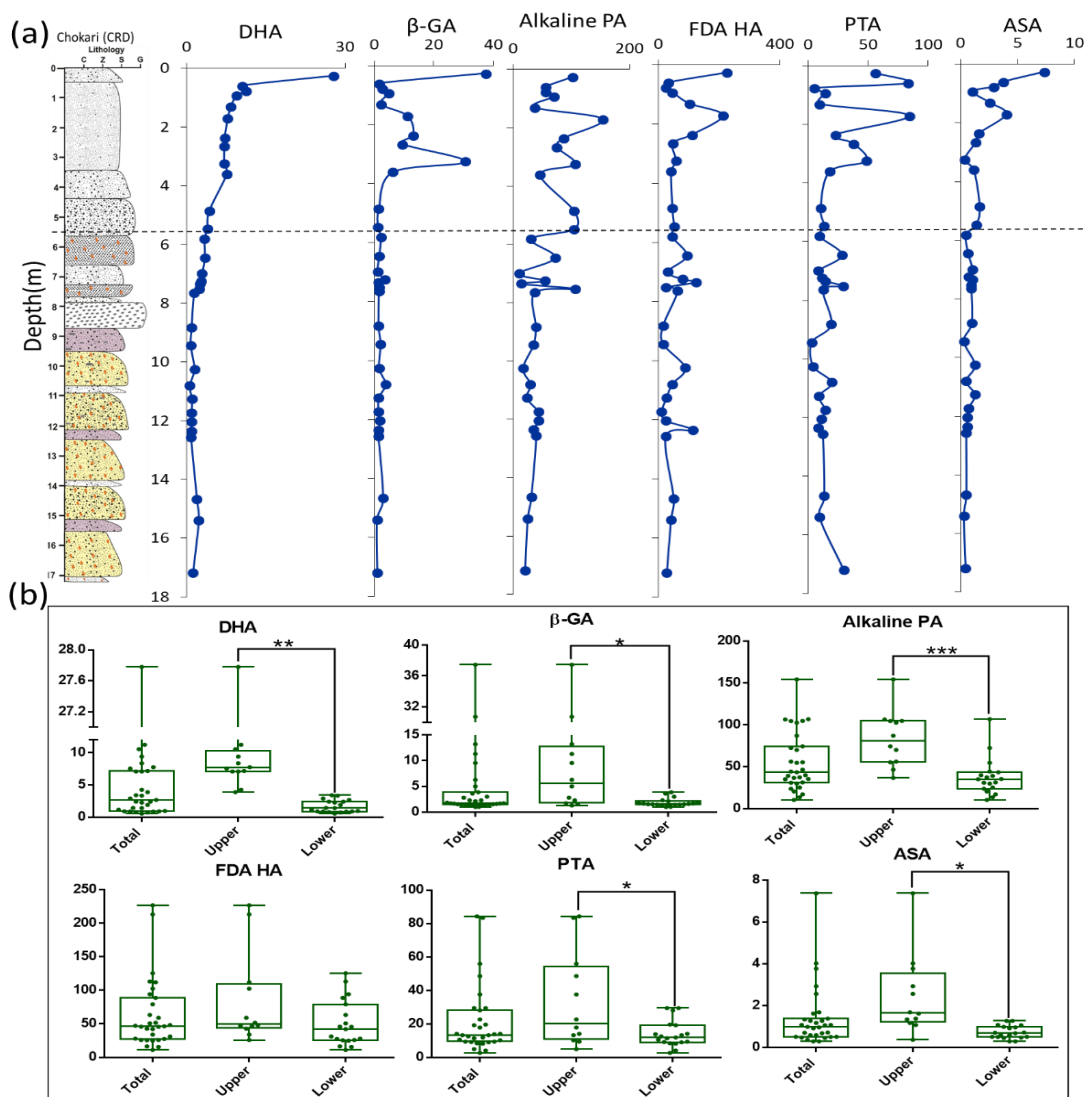


**Figure 3.3: Microbial enzyme activities within Chokari (CRD) core.** (a) A depth-wise pattern of activities. The dotted line demarcates the upper (up to ~5.5 m, Phase-II estuarine deposits) and lower (from ~5.5 to 17 m, Phase-I estuarine and fluvial deposits) regions of the core. (b) Box plots of the median and scatter values of enzyme activities of the upper and lower parts of the core. DHA: dehydrogenase activity ( $\mu\text{g TPF g}^{-1}$  dry wt core sediment  $24\text{h}^{-1}$ ),  $\beta$ -GA:  $\beta$ -D-glucosidase activity ( $\mu\text{g pNP g}^{-1}$  dry wt core sediment  $2\text{h}^{-1}$ ), Alkaline PA: alkaline phosphatase activity ( $\mu\text{g pNP g}^{-1}$  dry wt core sediment  $2\text{h}^{-1}$ ), FDA HA: fluorescein diacetate hydrolysis activity ( $\mu\text{g fluorescein g}^{-1}$  dry wt core sediment  $4\text{h}^{-1}$ ), PTA: protease activity ( $\mu\text{g tyrosine g}^{-1}$  dry wt core sediment  $2\text{h}^{-1}$ ), ASA: arylsulfatase activity ( $\mu\text{g pNP g}^{-1}$  dry wt core sediment  $2\text{h}^{-1}$ ) (\* $p < 0.05$ , \*\* $p < 0.01$ , \*\*\* $p < 0.001$ ; Welch's t-test).

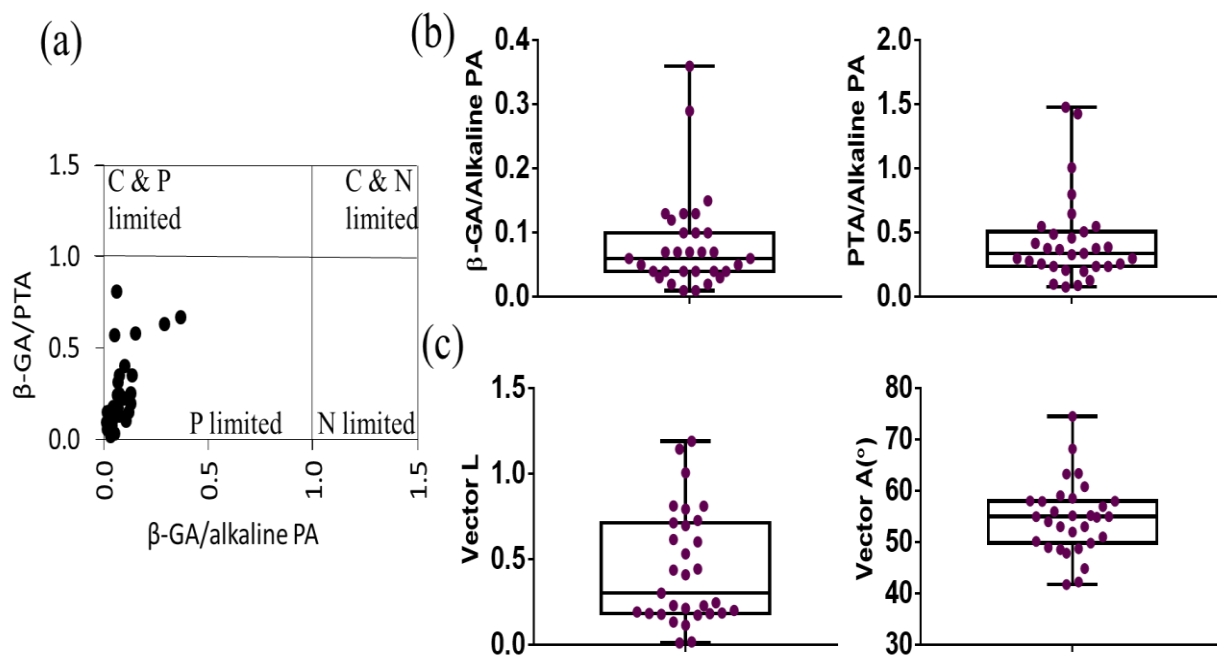


**Figure 3.4: Enzymatic stoichiometry within Chokari (CRD) core.** (a) Scatter plot of ecoenzymatic stoichiometry, with N cycle enzyme/P cycle enzyme (i.e.,  $\beta$ -GA/alkaline PA) as the x-axis and C cycle enzyme/ N cycle enzyme (i.e.,  $\beta$ -GA/PTA) as y-axis (b) Ratios of C cycle enzyme/ P cycle enzyme i.e.  $\beta$ -GA/Alkaline PA and N cycle enzyme/ P cycle enzyme i.e. PTA/Alkaline PA (c) vector analysis of ecoenzymatic stoichiometry: Vectors length (L, unitless) and vector angle (A, degree) calculated using formulas as shown below.

$$\text{Vector L} = \sqrt{(\ln\beta\text{-GA}/ \ln\text{PTA})^2 + (\ln\beta\text{-GA}/ \ln\text{Alkaline PA})^2}$$

$$\text{Vector A} = \text{Degrees} (\text{ATAN2} ((\ln\beta\text{-GA}/ \ln\text{Alkaline PA}), (\ln\beta\text{-GA}/ \ln\text{PTA})))$$

Therefore, here we determined culturable denitrifying bacterial counts and *nirS* gene (encoding cytochrome *cd*<sub>1</sub>-nitrite reductase - a key enzyme in denitrification) abundance. The denitrifying bacterial population was observed within the range of  $5.5 \times 10^2$  to  $6.2 \times 10^5$  per gram dry weight of sediment; however, it remains lower than heterotrophic counts in most samples (Fig. 3.5). The *nirS* gene copy numbers were found in the range of  $8.5 \times 10^4$  to  $5.93 \times 10^7$  per gram dry weight of sediment. Further, several studies reported the abundance and diversity of sulfate-reducing bacteria (Niu et al. 2018; Joulian et al. 2001) as well as the kinetics of microbial sulfate reduction in estuarine sediment (Pallud and Cappellen 2006). Thus, here we also

determined the abundance of the *dsrB* gene (encoding beta subunit of sulfite reductase - a key enzyme in sulfate reduction, hence used as a molecular marker for determining the abundance of sulfate reducing bacterial population) within the CRD estuarine core. The *dsrB* gene copy numbers were observed within the range of 0 (not detectable) to  $5.93 \times 10^7$  per gram dry weight of sediment in CRD core (Fig. 3.5).

*NirS* gene copy numbers were one to three orders of magnitudes lower than bacterial 16S rRNA gene copy numbers in CRD core samples (except top 0.25 m depth core sample which exhibits four orders of magnitudes lower *nirS* gene copy number than 16S rRNA gene copy numbers). *NirS* gene copy numbers were observed within the range of  $10^2$  to  $10^5$  per  $10^6$  16S rRNA gene copy numbers while *dsrB* gene copy numbers were observed within the range of 0 (not detectable) to  $10^4$  per  $10^6$  16S rRNA gene copy numbers (Fig. 3.5). As expected, copy numbers of the 16S rRNA gene were one to three orders of magnitudes higher than the observed culturable heterotrophic bacterial count. Likewise, *nirS* gene copy numbers were also one to three orders of magnitudes higher than observed culturable denitrifying bacterial count. Unlike enzyme activities, microbial abundance did not decrease with depth (Fig. 3.3, 3.5).

### 3.3.5 Correlation between and within microbiological and physicochemical parameters

Among microbial parameters, all enzyme activities clustered together on principle components suggesting that all enzyme activities were correlated significantly with each other in the CRD core (Fig. 3.6). Among physicochemical parameters, silt and clay content exhibited significant correlation with  $\text{Fe}_2\text{O}_3$ , MgO,  $\text{P}_2\text{O}_5$ , pH and salinity (Fig. 3.6). The correlation analysis between physicochemical properties of sediment and microbial parameters in the CRD core revealed that DHA and  $\beta$ -GA showed a significant positive correlation with org. C, pH, silt, clay,  $\text{Fe}_2\text{O}_3$ ,  $\text{P}_2\text{O}_5$ , MgO, Cu, as well as Zn content (Fig. 3.6, 3.7). Alkaline PA, PTA, and ASA also showed a significant positive correlation with  $\text{Fe}_2\text{O}_3$  and  $\text{P}_2\text{O}_5$ . All enzyme activities studied here exhibited a positive correlation with Cu, Zn, and pH. Sand content showed a significant negative correlation with DHA,  $\beta$ -GA, PTA, and ASA; sediment depth showed significant negative correlation with all the enzyme activities studied here while salinity showed a significant positive correlation with DHA and alkaline PA (Fig. 3.6, 3.7). Total heterotrophic count and 16S rRNA gene abundance exhibited a significant positive correlation only with Cu

and Zn content (Fig. 3.7). Denitrifiers count, *nirS*, and *dsrB* gene abundance did not show a significant correlation with any physicochemical parameters studied here (Fig. 3.6, 3.7).

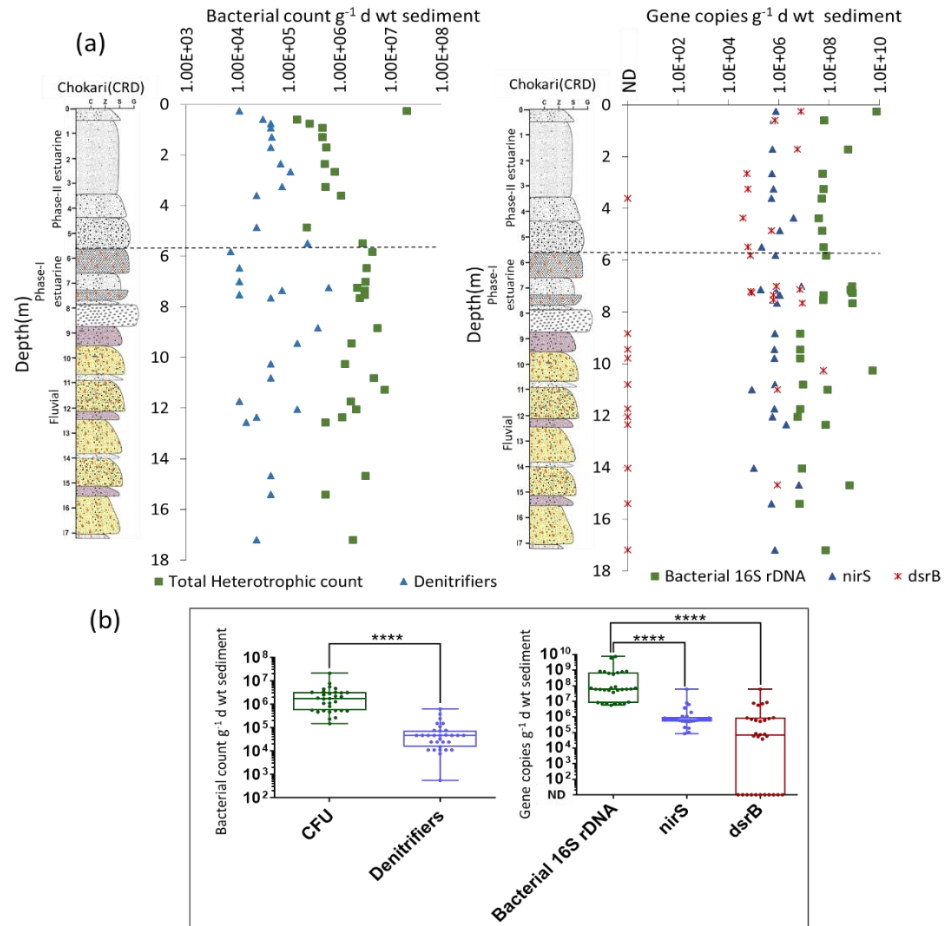


**Figure 3.5: Counts of culturable bacteria and gene abundance in CRD core samples. (a)** A depth-wise pattern of culturable bacterial counts and gene abundance. The dotted line demarcates the upper (up to ~5.5 m, Phase-II estuarine deposits) and lower (from ~5.5 to 17 m, Phase-I estuarine and fluvial deposits) regions of the core (b) Box plots of the median and scatter values of culturable bacterial counts and gene abundance. Culturable heterotrophic bacteria were determined by plating [colony-forming units (CFU)] and by denitrifiers were determined by MPN. The abundance of genes was determined by qPCR. Samples in which gene abundance was below detection limit represented at ND (not detected). The Wilcoxon signed-rank test (two-sided) was used to find significant differences between means of the culturable bacterial counts and gene abundances (\*\*\*\* $p < 0.0001$ ). Microbial abundance did not show significant difference between upper and lower region of core (Welch's t-test).

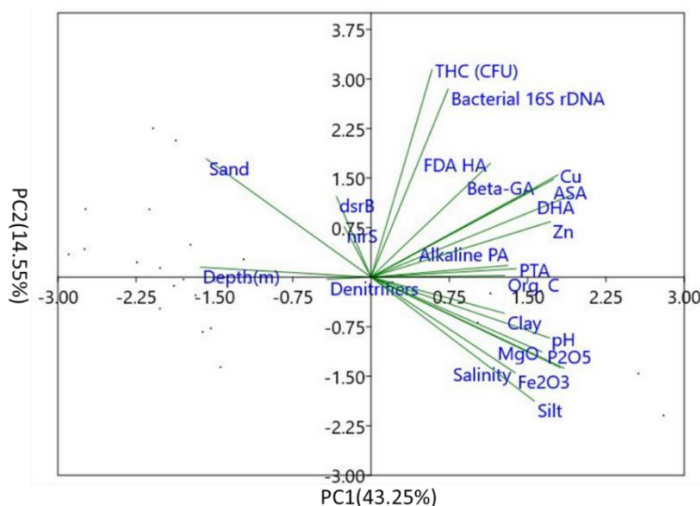


**Figure 3.6: Principal component analysis (PCA) between sediment depth, physicochemical characteristics and microbial parameters within CRD core.** DHA: dehydrogenase activity, Beta-GA:  $\beta$ -glucosidase activity, Alkaline PA: alkaline phosphatase activity, FDA HA: fluorescein diacetate hydrolysis activity, ASA: arylsulfatase activity, PTA: protease activity, B Bacterial 16S rDNA: Bacterial 16S rRNA gene, THC (CFU): total heterotrophic count (colony-forming units).

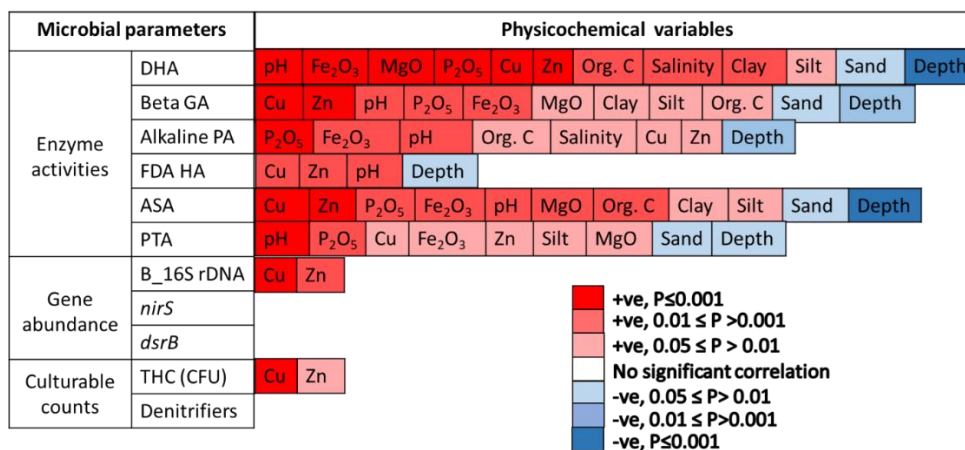


**Figure 3.7: Pearson correlation analysis between sediment depth, physicochemical parameters and microbial parameters**

DHA: dehydrogenase activity, Beta GA:  $\beta$ -glucosidase activity, Alkaline PA: alkaline phosphatase activity, FDA HA: fluorescein diacetate hydrolysis activity, ASA: arylsulfatase activity, PTA: protease activity, B\_16S rDNA: Bacterial 16S rDNA or Bacterial 16S rRNA gene, THC (CFU): Total heterotrophic count (colony-forming units).

### 3.3.6 Culturable bacterial diversity of CRD core samples

Abundant morphotypes of heterotrophic bacteria obtained from different subsurface horizons of the Chokari (CRD) core were identified by 16S rRNA gene sequencing. Phylum level distribution of the heterotrophic bacterial isolates showed them to represent *Actinobacteria*, *Proteobacteria*, *Bacteroidetes*, and *Firmicutes* (Fig. 3.8, Fig. A-III, Table 3.1). Their genus level identities (with >97% sequence similarity) (Table 3.1 and Fig. 3.8) showed that they belonged to 15 different genera. Among these, *Pseudomonas* was most abundant followed by *Rhizobium* and *Pseudarthrobacter* (Fig. 3.8). Phylogenetic relatedness between obtained bacterial isolates is represented in Fig. A-III (Appendix).

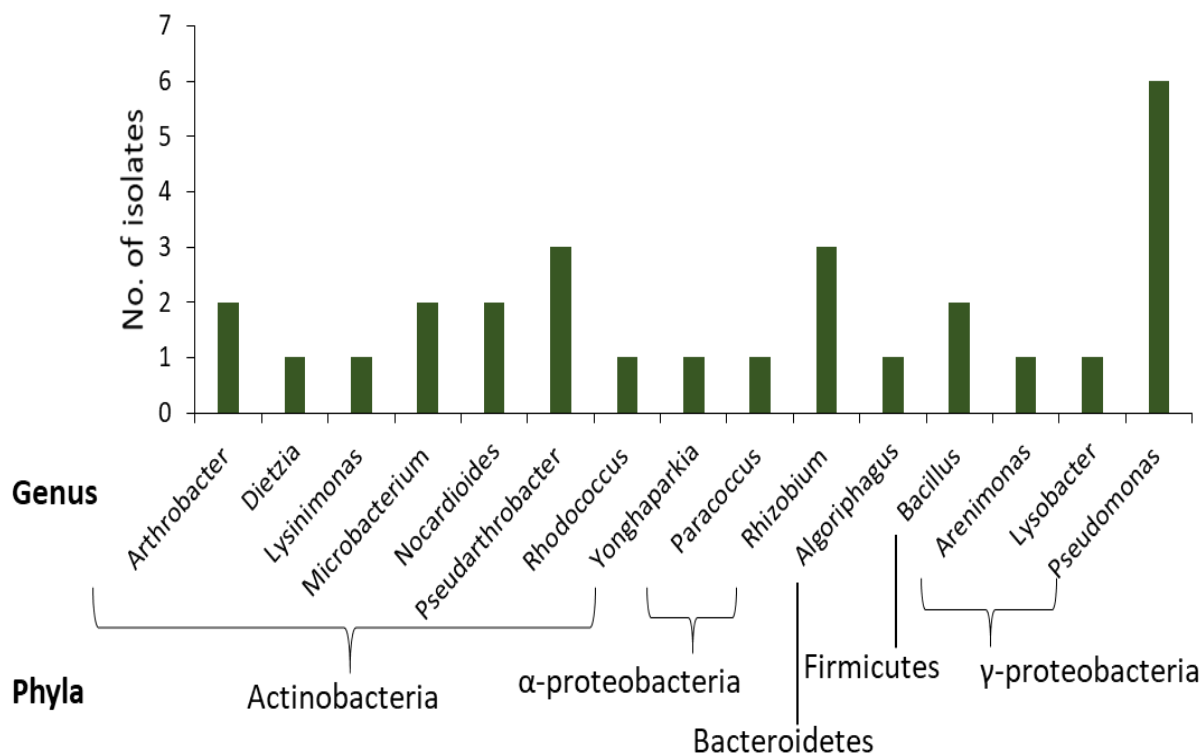


**Figure 3.8: Genus level identity (based on 16S rRNA gene partial sequence) of bacterial strains obtained from CRD core samples.** Total 28 isolates were obtained from different horizons (lithofacies) of CRD core among which the number of isolates affiliated with different genera is represented here together with their phyla level affiliation.

### 3.3.7 Microbial community profiling of CRD core samples by DGGE

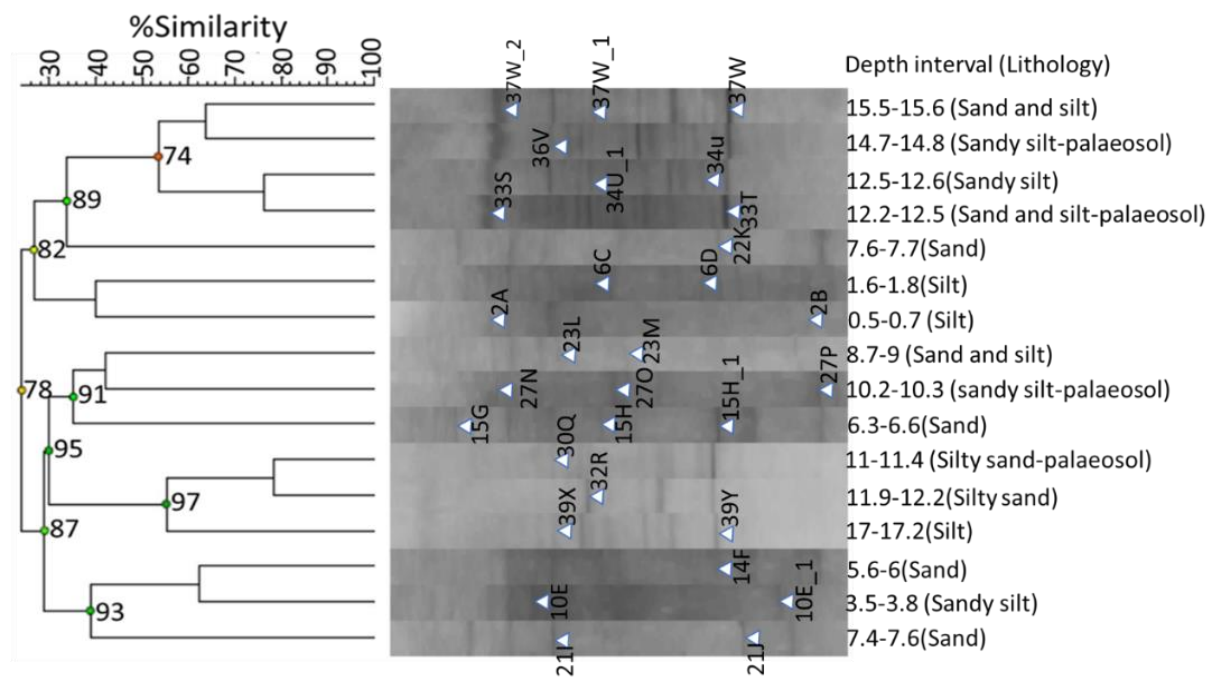
Microbial community profiling of sixteen representative samples from different horizons of Chokari (CRD) core revealed remarkable similarity between samples of different depths. The highest percentage similarity (i.e. 70-80%) in bacterial community profiling was observed between 12.2-12.5 m (palaeosol comprising an equal proportion of sand and silt) and 12.5-12.6 m (sandy silt) depth samples as well as 11-11.4 m (palaeosol comprising silty sand) and 11.9-12.2 m (silty sand) depth samples (Fig. 3.9). Sandy silt palaeosol observed at 14.7-14.8 m depth and 15.5-15.6 m depth sample comprising an equal proportion of sand and silt; 3.5-3.8 m depth sandy silt horizon and 5.6-6 m depth comprising sand had 60-70% similar bacterial community profiling. Palaeosol comprising sandy silt observed at depth 10.2-10.3 m showed only 40-50% bacterial community fingerprinting similarity with 8.7-9 m (comprising an equal proportion of sand and silt) (Fig. 3.9). Likewise, 1.6-1.8 m depth and 0.5-0.7 m depth silt horizons also exhibit 40-50% similarity in bacterial community fingerprinting. Paleosols observed in the CRD core were clustered distinctly depending on bacterial community profiling (Fig. 3.9). From DGGE community profiling, thirty representative bands (Fig. 3.9) were excised, cloned, and sequenced.

Figure 3.10 shows the taxonomic affiliation of these thirty bands based on the top ten best match sequences obtained in the NCBI-BLASTn similarity search. Table 3.2 represents percentage similarity and query coverage (with regards to topmost best match sequence obtained in NCBI-BLASTn similarity search) together with an accession number of bands. Among these 30 band sequences, 19 sequences exhibited affiliation with more than one taxonomic group because of the short length of the sequence (Fig. 3.10). However, the closest neighbors of the majority of the bands corresponded to organisms of the phylum *Proteobacteria* (87%), *Firmicutes* (7%), *Chloroflexi* (3%), and *Bacteroidetes* (3%) were observed in CRD core samples (Fig. 3.10a, 3.10b).

**Table 3.1: Genus level identification of bacterial isolates obtained from Chokari (CRD) sediment profile.**

Depth interval (m)	Lithology	Total count (CFU)*	CFU of identified isolate	Genus level identity of the bacterial isolate (GenBank accession number)	Phylum
0-0.5	Sandy silt	2.10×10 <sup>7</sup>	1.57×10 <sup>7</sup>	<i>Paracoccus</i> sp. CRD1.2B (MH311952)	α-Proteobacteria
0.5-0.7	Silt	1.47×10 <sup>5</sup>	9.82×10 <sup>4</sup>	<i>Pseudomonas</i> sp. CRD2.1A (MH311953)	γ-Proteobacteria
0.7-0.8	Silt	2.61×10 <sup>5</sup>	1.54×10 <sup>5</sup>	<i>Microbacterium</i> sp. CRD3.1A (MH311954)	Actinobacteria
1.2-1.4	Silt	4.63×10 <sup>5</sup>	1.50×10 <sup>5</sup>	<i>Bacillus</i> sp. CRD5.6F (MH311955)	Firmicutes
1.6-1.8	Silt	5.51×10 <sup>5</sup>	3.02×10 <sup>5</sup>	<i>Arthrobacter</i> sp. CRD6.3C (MH311956)	Actinobacteria
2.3-2.5	Silt	5.17×10 <sup>5</sup>	3.30×10 <sup>5</sup>	<i>Pseudomonas</i> sp. CRD7.1A (MH311957)	γ-Proteobacteria
2.6-2.8	Silt	8.11×10 <sup>5</sup>	3.58×10 <sup>5</sup>	<i>Rhizobium</i> sp. CRD8.7G (MH311958)	α-Proteobacteria
3.2-3.4	Silt	5.27×10 <sup>5</sup>	1.13×10 <sup>5</sup>	<i>Bacillus</i> sp. CRD9.4D (MH311959)	Firmicutes
3.5-3.8	Sandy silt	1.08×10 <sup>6</sup>	4.14×10 <sup>5</sup>	<i>Pseudomonas</i> sp. CRD10.3C (MH311960)	γ-Proteobacteria
5.3-5.6	Silty sand	2.82×10 <sup>6</sup>	2.11×10 <sup>6</sup>	<i>Rhodococcus erythropolis</i> CRD13.3C (MH311961)	Actinobacteria
5.7-6.0	Sand + Calcrete nodules	4.43×10 <sup>6</sup>	2.42×10 <sup>6</sup>	<i>Pseudarthrobacter</i> sp. CRD14.4D (MH311962)	Actinobacteria
6.3-6.6	Sand + Calcrete nodules	3.38×10 <sup>6</sup>	9.89×10 <sup>5</sup>	<i>Arenimonas</i> sp. CRD15.1A (MH311963)	γ-Proteobacteria
6.9-7.1	Sandy silt	3.22×10 <sup>6</sup>	9.71×10 <sup>5</sup>	<i>Algoriphagus</i> sp. CRD16.3C (MH311964)	Bacteroidetes
7.2-7.3	Sandy silt	2.22×10 <sup>6</sup>	1.86×10 <sup>6</sup>	<i>Nocardioides</i> sp. CRD19.3C (MH311965)	Actinobacteria
7.3-7.4	Sand + Calcrete nodules	3.09×10 <sup>6</sup>	2.34×10 <sup>6</sup>	<i>Lysobacter</i> sp. CRD20.1A (MH311966)	γ-Proteobacteria
7.4-7.6	Sand + Calcrete nodules	3.14×10 <sup>6</sup>	7.10×10 <sup>5</sup>	<i>Rhizobium</i> sp. CRD21.1A (MH311967)	α-Proteobacteria
7.6-7.7	Silty Sand	2.49×10 <sup>6</sup>	1.72×10 <sup>6</sup>	<i>Dietzia</i> sp. CRD22.4D (MH311968)	Actinobacteria
8.7-9.0	Sand and silt + Gravel	5.53×10 <sup>6</sup>	4.63×10 <sup>6</sup>	<i>Rhizobium</i> sp. CRD23.2B (MH311969)	α-Proteobacteria
9.3-9.6	Sand and silt + Gravel	1.72×10 <sup>6</sup>	8.01×10 <sup>5</sup>	<i>Pseudomonas</i> sp. CRD25.3C (MH311970)	γ-Proteobacteria
10.2-10.3	Sandy silt-Paleosol	1.28×10 <sup>6</sup>	7.21×10 <sup>5</sup>	<i>Nocardioides</i> sp. CRD27.1A (MH311971)	Actinobacteria
10.8-10.9	Sandy silt	4.71×10 <sup>6</sup>	2.20×10 <sup>6</sup>	<i>Pseudomonas</i> sp. CRD28.3C (MH311972)	γ-Proteobacteria
11.2-11.3	Silty sand-Paleosol	7.70×10 <sup>6</sup>	4.60×10 <sup>6</sup>	<i>Pseudarthrobacter</i> sp. CRD30.3C (MH311973)	Actinobacteria
11.6-11.9	Silty sand - Paleosol	1.67×10 <sup>6</sup>	7.69×10 <sup>5</sup>	<i>Yonghaparkia</i> sp. CRD31.1A (MH311974)	Actinobacteria
11.9-12.2	Silty sand - Paleosol	2.11×10 <sup>6</sup>	8.30×10 <sup>5</sup>	<i>Arthrobacter</i> sp. CRD32.2B (MH311975)	Actinobacteria
12.2-12.5	Sand and silt	1.12×10 <sup>6</sup>	3.35×10 <sup>5</sup>	<i>Microbacterium</i> sp. CRD33.1A (MH311976)	Actinobacteria
12.5-12.6	Sandy silt - Paleosol	5.33×10 <sup>5</sup>	2.72×10 <sup>5</sup>	<i>Pseudomonas</i> sp. CRD34.2B (MH311977)	γ-Proteobacteria
14.7-15	Sandy silt - Paleosol	3.22×10 <sup>6</sup>	8.99×10 <sup>5</sup>	<i>Lysinimonas</i> sp. CRD36.3C (MH311978)	Actinobacteria
15.3-15.6	Sand and silt	5.35×10 <sup>5</sup>	3.32×10 <sup>5</sup>	<i>Pseudarthrobacter</i> sp. CRD37.5E (MH311979)	Actinobacteria

\*Colony-forming units (CFU) expressed as bacterial counts per g dry weight of sediment.



**Figure 3.9: 16S rDNA PCR-DGGE clustering of microbial communities of the CRD core samples.** Sample relatedness was analysed by the Dice similarity coefficient and unweighted pair group method with arithmetic means algorithm (UPGMA) clustering. Values at the nodes represent cophenetic correlations. Samples are denoted in terms of depth intervals (in m) and corresponding lithological horizons (described in parentheses).

### 3.3.8 Microbial diversity assessment of CRD core samples by Illumina sequencing

Amplicon analysis of the V3-V4 region of the 16S rRNA gene by Illumina sequencing was performed for three representative core samples includes 0.5-0.7 m depth sample (CRD 2), 1.6-1.8 m depth sample (CRD 6), and 10.2 to 10.3 m depth sample (CRD 27). The location of selected samples within CRD litholog is depicted in Fig. 3.11a. Based on relative microbial enzyme activities and 16S rRNA gene copy numbers these three representative core samples were selected to determine an in-depth study of microbial community composition (Table 3.3).

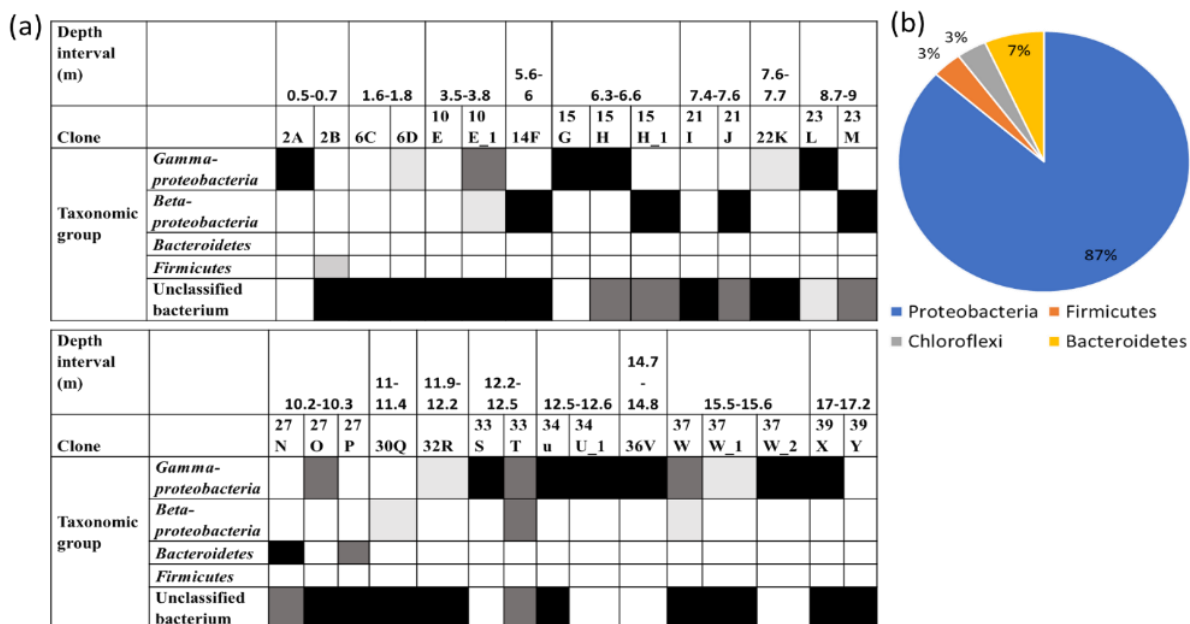


**Figure 3.10: Taxonomic affiliation of DGGE band sequences (based on NCBI-BLASTn) obtained from CRD core samples** (a) Taxonomic affiliation of DGGE band sequences represented by top ten BLASTn based sequence homology search. Black color denotes phyla level affiliation shown by  $\geq 5$  homologous sequences from top 10 best matches, dark grey color denotes phyla level affiliation shown by 2 to 4 homologous sequences from top 10 best matches, light grey color denotes phyla level affiliation shown by only one homologous sequences from top 10 best matches and white color denotes no sequence similarity obtained for that phyla in top 10 best matches. (b) Pie chart representing the percentage of phyla distribution within DGGE band sequences

After preprocessing of raw reads, a total of 642462 reads were obtained from three samples and a total of 32763 OTUs were obtained from these preprocessing reads after singleton OTU removal (Table 3.4). Among 32763 OTUs, only 1304 OTUs were common between all three samples; 4014 OTUs were common between CRD 2 and CRD 6; 2189 OTUs were common between CRD 2 and CRD 27; and 696 OTUs were common between CRD 6 and CRD 27 (Fig. 3.11a). A total of 11752 unique OTUs were observed within CRD 2, while within CRD 6 9863 unique OTUs and in CRD 27 2945 unique OTUs were observed (Fig. 3.11a). A total of 1304 shared OTUs encompassed 27.1% of total reads in CRD 2, 14.9% of total reads in CRD 6, and 67.3% of total reads in CRD 27 (Fig. 3.11b).

**Table 3.2: Sequence analysis of selected DGGE bands obtained from CRD core samples based on topmost best match sequence acquired in NCBI-BLASTn similarity search.**

Depth interval (m)	CRD-DGGE band	NCBI accession number	Topmost closely related sequence in NCBI (Accession number)	Query coverage (%)	Similarity (%)
0.5-0.7	2A	MK156174	<i>Pseudomonas aeruginosa</i> strain EMSB 21 (MH001386)	100	100
	2B	MK156175	Uncultured bacterium clone ZLL-E80 (JF807034)	100	96.89
1.6-1.8	6C	MK156176	Uncultured bacterium clone garden_soil_5229 (KP153890)	100	100
	6D	MK156177	<i>Immirania thermoithophila</i> strain S2479 (NR_148577)	100	94.27
3.5-3.8	10E	MK240488	Uncultured microorganism clone SGGSWU6 (KX925226)	99	100
	10E_1	MK241795	Uncultured bacterium clone 16S_MJ4_02(KC925138)	100	100
5.6-6	14F	MK156178	Uncultured bacterium clone LIB066_B_D02 (KM851839)	99	98.95
6.3-6.6	15G	MK156179	<i>Pseudomonas</i> sp. strain V5R.11 (MK138854)	100	99.48
	15H	MK156180	<i>Acinetobacter junii</i> strain FC2961 (MK089549)	100	99.47
	15H_1	MK241794	<i>Limnobacter thiooxidans</i> strain T369_AW6 (MF193784)	100	99.44
7.4-7.6	21I	MK156181	Uncultured bacterium clone OTU3 (KX380998 )	100	100
	21J	MK156182	<i>Limnobacter</i> sp. strain LZ-4 (MK100324)	100	100
7.6-7.7	22K	MK240489	<i>Rheinheimera</i> sp. strain B19 (MK182920)	100	100
8.7-9	23L	MK156183	<i>Acinetobacter junii</i> strain LH-1-1 (MK053916)	100	100
	23M	MK156184	Uncultured bacterium clone nbw304b10c1 (GQ087573)	100	100
10.2-10.3	27N	MK156185	<i>Flavobacterium</i> sp. strain MMS16-B30 (MF289262)	100	100
	27O	MK156186	Uncultured <i>Rheinheimera</i> sp. clone 9EP3 (KX270189)	100	100
	27P	MK156187	<i>Confluentibacter citreus</i> strain XJNY (NR_158095)	100	98.88
11-11.4	30Q	MK156188	Uncultured bacterium clone BAS1082 (KF379684)	99	100
11.9-12.2	32R	MK156189	<i>Rheinheimera</i> sp. strain B19 (MK182920)	99	99.47
12.2-12.5	33S	MK156190	<i>Pseudomonas</i> sp. strain R35 (MH773397)	100	100
	33T	MK156191	Uncultured bacterium clone 16S_MJ4_02 (KC925138)	100	100
12.5-12.6	34u	MK156192	<i>Halomonas aquamarina</i> strain NIOSSD026#86 (MH255343)	100	99.48
	34U_1	MK241793	<i>Rheinheimera</i> sp. R083 (KC252917)	100	100
14.7-14.8	36V	MK156193	<i>Pseudomonas</i> sp. strain C56 (MK182919)	100	99.48
15.5-15.6	37W	MK156194	Uncultured Gamma -proteobacterium clone: DG-KL- G5 (AB635929)	100	99.48
	37W_1	MK241791	<i>Rheinheimera</i> sp. strain B19 (MK182920)	98	99.48
	37W_2	MK241792	<i>Pseudomonas otitidis</i> isolate AAI-4 (LN558608)	100	100
17-17.2	39X	MK156195	Uncultured <i>Cellvibrio</i> sp. clone FR28 (KY969318)	98	100
	39Y	MK156196	Uncultured bacterium clone LSZ-B-80 (KR089614)	100	99.47

**Table 3.3: Mean, SD, and Max values of enzyme activities and 16S rRNA gene copy numbers of CRD core samples selected for metabarcoding and 0.2-0.3 m core sample (CRD 1).**

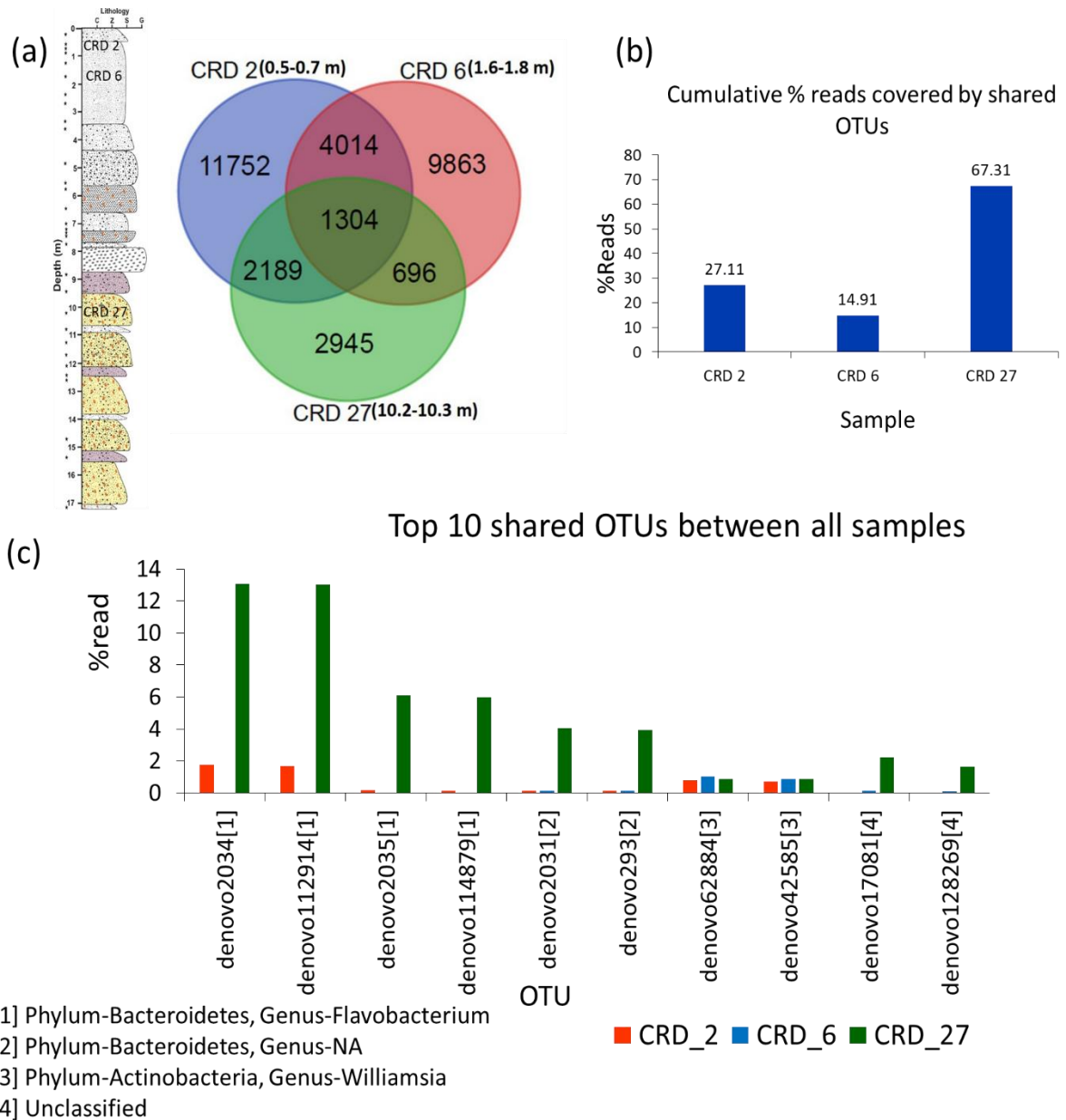
Sample detail		Enzyme activities						Gene copies
Depth interval (m)	Lithological description	DHA	$\beta$ -GA	Alk PA	FDA HA	PTA	ASA	16S rRNA gene
0.2-0.3 (CRD 1)	sandy silt	27.78	37.5	102.6	226.5	55.95	7.37	7.50×09
0.5-0.7 (CRD 2)	Silt	10.54	1.73	56.2	33.9	83.42	3.76	6.17×07
1.6-1.8 (CRD 6)	silt	7.75	11.3	154.2	213.1	84.32	4.02	5.56×08
10.2 -10.3 (CRD 27)	sandy silt (palaeosols)	1.44	1.69	17.1	88.6	4.16	1.27	5.93×09
	<b>Mean</b>	4.64	5.13	55.2	63.2	21.53	1.39	6.47×08
	<b>SD</b>	5.39	8.34	34.9	52.03	20.70	1.45	1.69×09
	<b>Max</b>	27.78	37.45	154.2	226.5	84.32	7.37	7.50×09

- SD: standard deviation, Max: maximum, Abbreviations and units of microbial parameters described in the text.
- See Fig. 3.3 and 3.5 for microbial parameters of the complete core. Core samples CRD 1, CRD 2, and CRD 6 lie within estuarine deposits while CRD 27 lies within fluvial deposits. Sample CRD 2, CRD 6, and CRD 27 were selected for metabarcoding.

**Table 3.4: Total number of reads and OTUs obtained after preprocessing**

	CRD 2	CRD 6	CRD 27	Total
Total Reads	203856	259520	179106	642462
Total OTUs Picked	81328	48801	15764	138362
Total Singleton OTUs	65145	35837	10620	105599
Total OTUs after Singleton removal	16183	12964	5144	32763

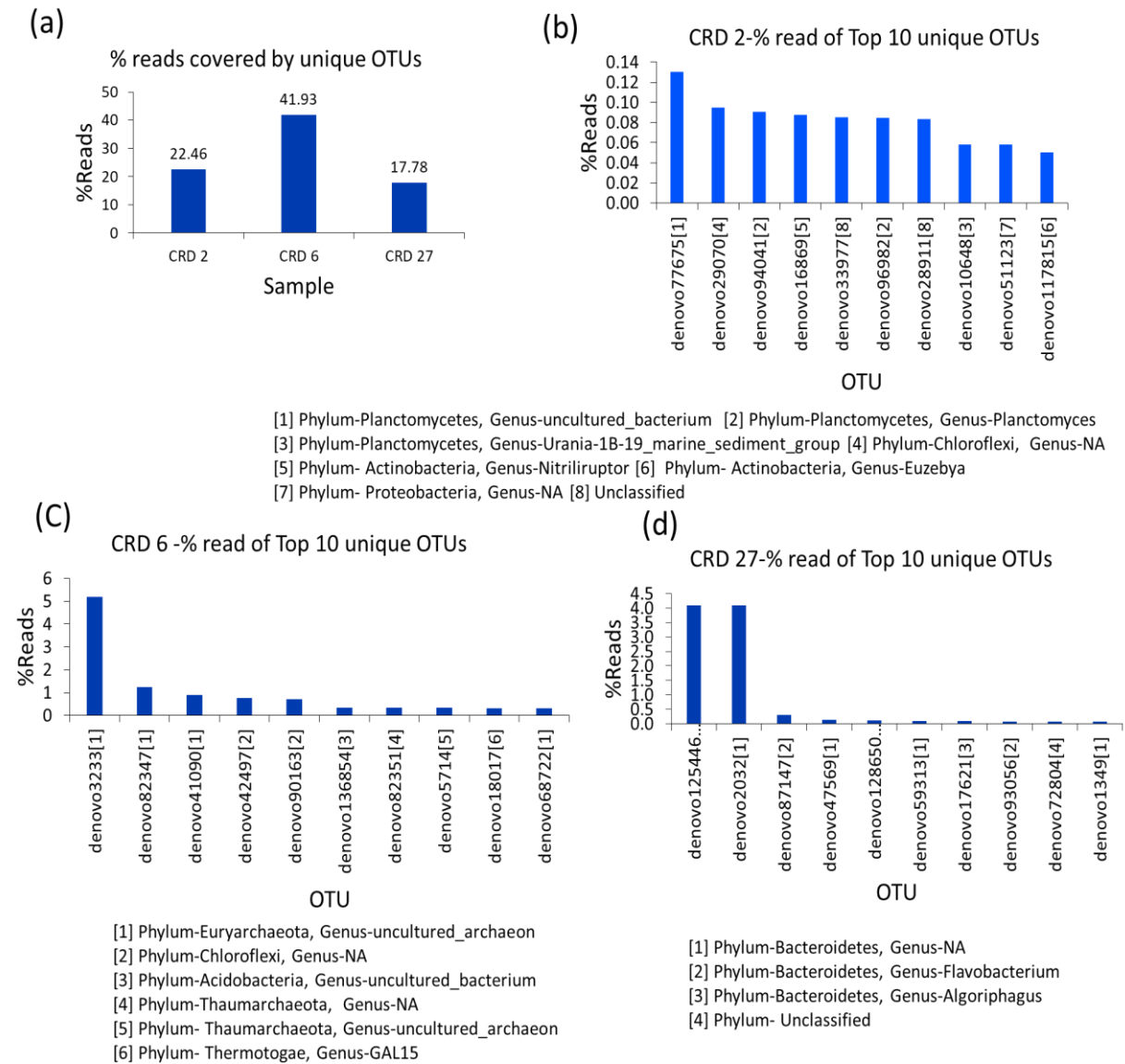
Among 1304 shared OTUs between all three samples, the top 10 shared OTUs cumulatively encompassed 5.64% of total reads in CRD 2, 2.44% of total reads in CRD 6, and 51.8% of total reads in CRD 27. Among the top 10 shared OTUs, the first six are affiliated with the phyla Bacteroidetes, two are affiliated with Actinobacteria, and the remaining two are unclassified (Fig. 3.11c).



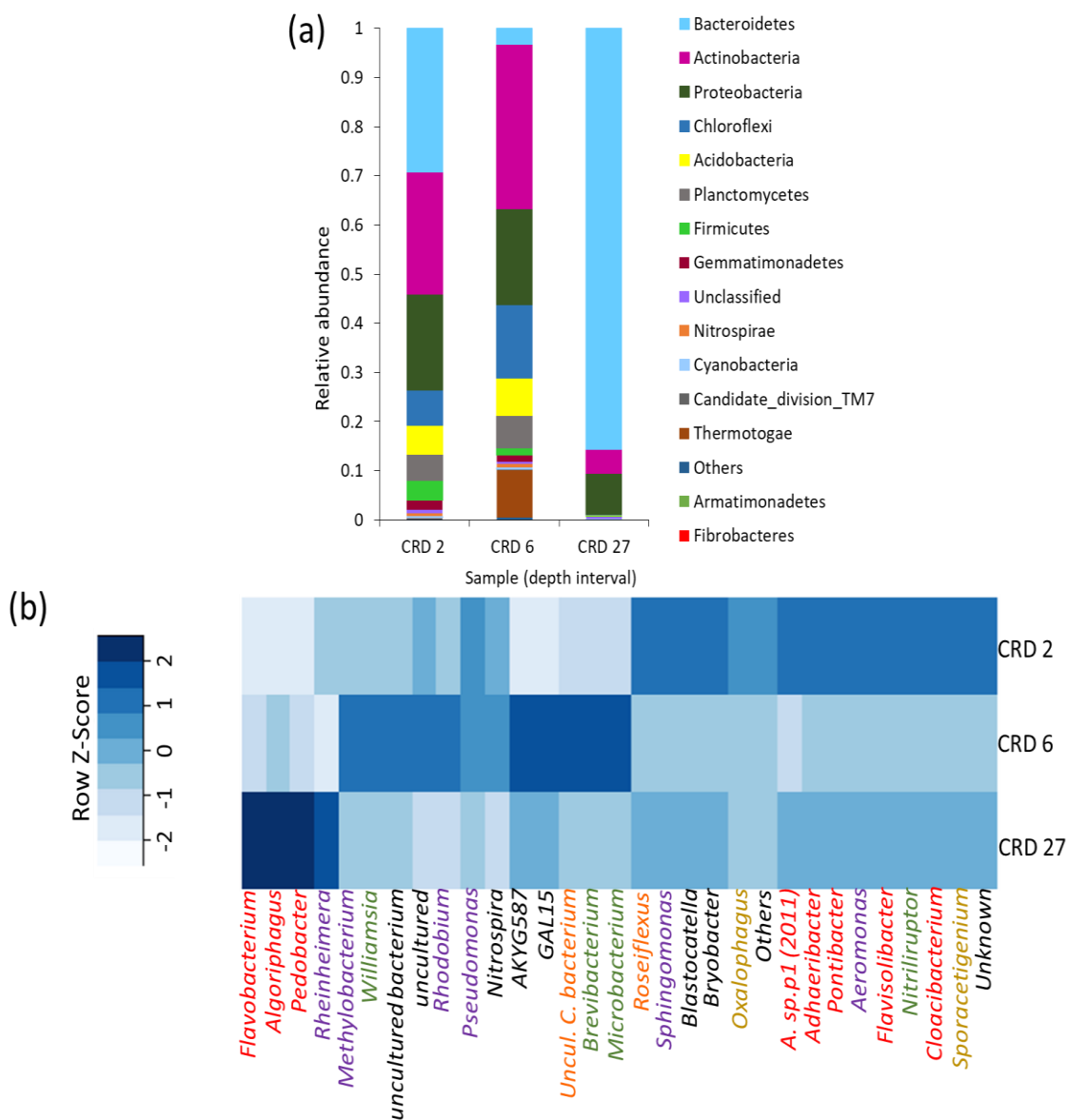
**Figure 3.11: Distribution of OTUs, cumulative percentage reads encompassed by shared OTUs and taxonomic affiliation of top 10 shared OTUs.** (a) Lithology of CRD core denoted with a metabarcoding sample location and Venn diagrams of the presence and absence of OTUs as well as shared OTUs (b) Cumulative percentage reads encompassed by shared OTUs (c) percentage reads encompassed by top 10 shared OTUs and their taxonomic affiliation. A number denoted in square parenthesis after OTU number represent their taxonomic affiliation mention below the figure. NA: Not Assigned.

Figure 3.12a represents the percentage of reads encompassed by unique OTUs of all three samples. A total of 22.46% of reads are encompassed by unique OTUs observed in CRD 2, a total of 41.93% of reads are encompassed by unique OTUs observed in CRD 6, and a total of 17.78% of reads are encompassed by unique OTUs observed in CRD 27. Figure 3.12b, 3.12c, and 3.12d show the percentage of reads covered by the top 10 unique OTUs in each sample and their taxonomic affiliation. In CRD 2, the top 10 unique OTUs are largely affiliated with the bacterial phyla Planctomycetes, Chloroflexi, Actinobacteria, and Proteobacteria (Fig.3.12b). In CRD 6, the top 10 unique OTUs are largely affiliated with the Euryarchaeota phyla (Fig. 3.12c). In CRD 27, the top 10 unique OTUs are largely affiliated with the Bacteroidetes phyla (Fig. 3.12d).

Microbial community composition was different between the three samples at the phylum level. *Bacteroidetes* (86% within CRD 27, 2% within CRD 6, 29% within CRD 2), *Actinobacteria* (5% within CRD 27, 21% within CRD 6, 24% within CRD 2), *Proteobacteria* (8% within CRD 27, 12% within CRD 6, 19% within CRD 2), *Chloroflexi* (0.13% within CRD 27, 9% within CRD 6, 7% within CRD 2), and *Acidobacteria* (0.13% within CRD 27, 5% within CRD 6, 6% within CRD 2) were most abundant top five phyla observed in CRD samples (Fig. 3.13a). The bacterial community belongs to the phyla *Planctomycetes*, *Thermotogae*, *Firmicutes*, *Gemmatimonadetes*, *Nitrospirae*, *Cyanobacteria*, *Candidate division TM7*, *Fibrobacteres*, and *Armatimonadetes* were also observed within the CRD core samples (Fig. 3.13a). The heatmap of taxonomy comparison analysis at the genus level showed a higher abundance of *Algoriphagus*, *Flavobacterium*, *Pedobacter*, and *Rheinheimera* within the CRD 27 sample as compared to the CRD 6 and CRD 2 samples (Fig. 3.13b). A higher abundance of the genus *Methylobacterium*, *Williamsia*, *Rhodobium*, AKYG587, GAL15, *Brevibacterium*, and *Microbacterium* was observed within CRD 6 as compared to CRD 2 and CRD 27. Likewise, a higher abundance of genera *Roseiflexus*, *Sphingomonas*, *Blastocatella*, *Bryobacter*, *Algoriphagus* sp.p1 (2011), *Adhaeribacter*, *Pontibacter*, *Aeromonas*, *Flavisolibacter*, *Nitriliruptor*, *Cloacibacterium*, and *Sporacetigenium* was observed within CRD 2 as compared to the other two core samples (Fig. 3.13b).



**Figure 3.12: Cumulative percentage reads encompassed by shared OTUs and percentage reads covered by the top 10 unique OTUs and their taxonomic affiliation.** (a) Cumulative percentage of reads encompassed by shared OTUs (b) proportion of reads covered by the top ten unique CRD 2 OTUs and their taxonomic affiliation (c) proportion of reads covered by the top ten unique CRD 6 OTUs and their taxonomic affiliation (d) proportion of reads covered by the top ten unique CRD 27 OTUs and their taxonomic affiliation. A number denoted in square parenthesis after the OTU number represents their taxonomic affiliation, mentioned below in each figure. NA: Not Assigned.



**Figure 3.13: Distribution of bacterial taxa within Chokari (CRD) core samples.** (a) Distribution of the 15 most abundant phyla (b) Heatmap of relative abundance (percent) of 30 abundant bacterial genera. The heat map scale displays the row Z score (actual relative abundance of genus- mean relative abundance/ standard deviation). Color coding represents the phylum to which each genus belongs, as follows: *Bacteroidetes* in red, *Proteobacteria* in purple, *Actinobacteria* in green, *Chloroflexi* in orange, *Firmicutes* in golden yellow, and the remaining other genus are in black.

### **3.3.9 Functional profile analysis of CRD core samples**

Functional prediction from microbial community composition of CRD core samples obtained by Illumina sequencing indicates that ammonium oxidizers are most dominant in all three samples. However, within CRD 27 the highest percentage (74.4%) of the microbial community was able to oxidize ammonia while within CRD 6 67.6% microbial population and within CRD 2 46.8% microbial population was able to oxidize ammonia (Fig. 3.14). The core sample CRD 27 had a relatively higher percentage of microbial population that was able to do dehalogenation (70.8%) and sulfide oxidation (67.8%) as compared to CRD 6 and CRD 2 samples (Fig. 3.14). At 10.2-10.3 m (CRD 27) depth core sample 20.9% sulfate reducers, 17.6% nitrite reducers, and 12.6% nitrogen-fixing bacterial population were also observed.

Among microbial population present at 0.5-0.7 m depth (CRD 2) core sample, greater than 20% of the bacterial population was able to carry out nitrite reduction (22.3%), sulfate reduction (27.3%), dehalogenation (26%), and sulfide oxidation (27%). In 1.6-1.8 m depth (CRD 6) core sample 18.4% sulfate reducer, 14.1% nitrite reducer, 10.3% sulfide oxidizer, 8.6% xylan degrader, 5.5% atrazine metabolizing bacteria, and 12.8% microbial population involved in dehalogenation was present (Fig. 3.14). Sulfur oxidizer, sulfur reducer, naphthalene degrading, aromatic hydrocarbons degrading microbial community also present in CRD core samples at lower abundance (Fig. 3.14). Inclusive, the functional profile of CRD core samples indicates that ammonium oxidizers, atrazine metabolizing bacteria, nitrite reducer, nitrogen-fixing bacteria, sulfate reducer, sulfide oxidizer, xylan degrader, and bacteria that carried out dehalogenation are prominent in CRD core samples.

## **3.4 Discussion**

### **3.4.1 Sediment stratigraphy and microbial characteristics within CRD core**

Stratigraphic sequences observed in the CRD core are comparable to the sediment deposits described from other parts of the Mahi River basin. For instance, the estuarine sediment deposits observed within the CRD core are comparable to the exposed (cliff) estuarine sediments located at Kothiyakhad on the opposite bank of the river (Kusumgar et al. 1998; Raj

et al. 1999). The fluvial sediment deposits observed in the CRD core beneath the estuarine deposits is lithologically comparable to the Late Pleistocene sediment deposits observed in exposed cliff sections of the older terrace of the Mahi River basin suggesting an influence of regional phases of sedimentation and pedogenesis (Maurya et al. 1997a, 2000; Juyal et al. 2000).

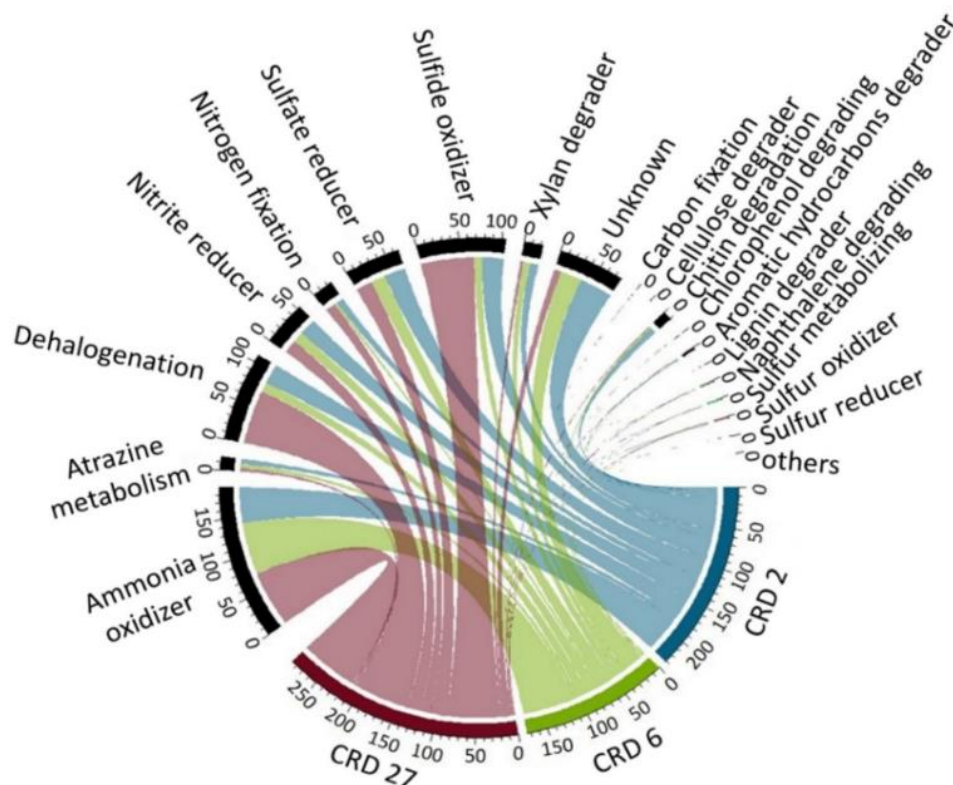


**Figure 3.14: Circos plot of CRD core samples displaying percentage distribution of different functional groups of bacteria based on METAGENassist prediction tool.**

Enzyme activities observed throughout the 17 m depth of CRD core indicates the essential role of the CRD estuarine ecosystem in C, N, P, and S biogeochemical cycling. Recently, coenzymatic stoichiometry has been suggested as a useful indicator of the microbial resource limitation in different regions or ecosystems since extracellular enzyme activity reflects the microbial response to whether the available environmental resources can meet its metabolic demands (Hill et al. 2014; Sinsabaugh et al. 2009). Coenzymatic stoichiometry analysis indicated P limitation in CRD core. P deficiency is common in the terrace (older) sediments due to the combination of available P and base cations, especially Ca as Ca will react

with P to form insoluble precipitates in calcareous soils or sediments (Iyamuremye and Dick 1996). This might be the reason for the microbial P limitation in the studied region.

In this study, we also reported the presence of a sustainable number of culturable heterotrophic bacteria throughout the 17 m deep Mahi River estuarine core. Balkwill (1989) and Zlatkin et al. (1996) reported the presence of cultivable bacteria in deep subsurface sedimentary ecosystems of Savannah River Plant (SRP, Carolina) and San Juan basin (Cerro Negro, New Mexico) respectively. Zhou et al. (2017) revealed the presence of  $10^8$  to  $10^{10}$  16S rRNA gene copies per gram dry sediment up to ~0.5 m depth within intertidal mudflats and mangrove forest located at Shenzhen River estuary and Hong et al. (2019) revealed the presence of  $\sim 10^9$  16S rRNA gene copies per gram of sediment up to the depth of 1 m within the subterranean estuary. Here we reported the presence of  $\sim 10^6$  to  $10^9$  bacterial 16S rRNA gene copy numbers per gram dry weight of sediment up to depth 17 m in the Mahi River estuarine core. The abundance of denitrifying and sulfate-reducing prokaryotes was also determined here by quantifying functional gene *nirS* (used to determine the abundance of the denitrifying population) and *dsrB* (used to determine the abundance of the sulfate-reducing population) via qPCR. Denitrification [reduction of nitrate ( $\text{NO}_3^-$ ) or nitrite ( $\text{NO}_2^-$ ) into the various N gases] and sulfate reduction are primary metabolic processes that occur in subsurface sedimentary environments (Lovley and Chapelle 1995). Mosier and Francis (2010) reported the presence of  $5.4 \times 10^5$  to  $5.4 \times 10^7$  *nirS* copies in the San Francisco Bay estuary surface sediment samples, Zeleke et al. (2013) described the presence of  $5.4 \times 10^5$  to  $5.4 \times 10^7$  *dsrB* copies in the mudflat sediments collected up to ~1 m depth from Yangtze River estuary (China). Here we reported the presence of  $8.5 \times 10^4$  to  $5.93 \times 10^7$  *nirS* gene copies (i.e. 0.01-10% of the total 16S rRNA gene copies) and not detectable to  $5.93 \times 10^7$  gene copies of the *dsrB* gene (i.e. 0-1.2% of the total 16S rRNA gene copies) in the 17 m deep Chokari (CRD) estuarine core. Culturable denitrifying bacteria were also detected throughout 17 m in the CRD core.

Subsurface sediments possess a physically and chemically complex oligotrophic environment because of this subsurface sedimentary ecosystems comprise physiologically and phylogenetically highly diverse microbes. Here we also carried out microbial diversity assessment of Chokari (CRD) core samples by traditional isolation based method, by DGGE, and by Illumina sequencing. The cultivation based approach is still important because it

provides insight into the physiological capacities of microbes which are necessary to understand the ecological functioning of bacterial species in the environment (Fry 2000). In the cultivation based approach many of the bacteria recovered from CRD core samples are facultative anaerobic bacteria (e.g. *Nocardioides* sp., *Paracoccus* sp., *Bacillus* sp., *Lysobacter* sp., *Pseudomonas* sp.). The dominance of isolates belonging to *Actinobacteria*, *Proteobacteria*, *Bacteroidetes*, and *Firmicutes* phyla was observed in CRD core samples which reflected due to the ease in the cultivation of isolates belonging to these phyla (Hugenholtz 2002). Additionally, DGGE analysis revealed the presence of a bacterial population belonging to *Proteobacteria*, *Firmicutes*, *Chloroflexi*, and *Bacteroidetes* phyla in CRD core samples. Likewise, the metabarcoding study also revealed a greater abundance of phyla *Bacteroidetes*, *Actinobacteria*, *Proteobacteria*, *Chloroflexi*, and *Acidobacteria* in CRD core samples. Other studies also reported dominance of bacterial phyla *Proteobacteria*, *Actinobacteria*, *Bacteroidetes*, *Firmicutes*, *Chloroflexi*, and *Acidobacteria* in subsurface tidal-flat and estuary sediments (Wilms et al. 2006; Hong et al. 2019). Functional prediction of microbial community obtained by metabarcoding analysis revealed that microbial populations present in CRD core samples were able to carry out ammonia oxidation, nitrite reduction, sulfate reduction, sulfide oxidation, and dehalogenation (Fig. 3.14). These metabolic activities are foremost in tidal-flat or estuarine sedimentary ecosystems (Mosier and Francis 2008; Jiang et al. 2009; Zanaroli et al. 2015; Baker et al. 2015). On the whole, microbial enzyme activities, metabarcoding based functional prediction, qPCR based detection of *nirS* and *dsrB* gene copies, presence of culturable denitrifying bacterial population within CRD core samples emphasize the role of CRD estuarine ecosystem in C, N, and S cycling.

### **3.4.2 Impact of sediment physicochemical properties on microbial parameters**

Among environmental factors studied here, total org. C content and sediment pH showed a positive impact on microbial enzyme activities. Moreover, sediment pH can serve as the best predictor for PTA in the CRD core. Various earlier studies also reported a significant positive relationship of total org. C content and pH with microbial enzyme activities (Sinsabaugh et al. 2008; Subrahmanyam et al. 2011a; Polyak et al. 2017) and soil pH as the best predictor for several microbial enzyme activities (Sinsabaugh et al. 2008). The effect of salinity

on microbial activity varies depending on the site-specific availability of ions and the type of enzyme (Pan et al. 2013; Frankenberger and Bingham 1982). Morrissey et al. (2014) reported a positive correlation of salinity with microbial enzyme activities in tidal wetlands while Hu et al. (2014) reported a negative impact of salinity on microbial enzyme activities in coastal and riparian wetlands of the Yangtze River estuary. Here, we have observed the positive impact of salinity on DHA and alkaline PA. Further, a negative correlation of sand content and moderate positive correlation of silt and clay content with microbial parameters observed within CRD core is in accordance with the result reported by Albrechtsen and Winding (1992) for glacio-fluvial Quaternary sediments. This might be reflected due to the lower capability of sand particles for organic matter adsorption, moisture retention, extracellular enzyme or protein adsorption than fine particles such as silt and clay (Oades 1988; Nannipieri et al. 2002).

Among elemental analyses studied here, Mg, Fe, P (measured in form of their oxides), Cu, and Zn had a strong positive correlation with several microbial parameters in the CRD core. The positive correlation of Mg, Fe, P oxides with microbial enzyme activities is consistent with Sudhakaran et al. (2019). Negative influence or adverse effect of various trace elements such as Cu and Zn on soil/sediment microbial parameters has been reported in earlier studies (Hattori 1992; Jaiswal and Pandey 2018). Contradictory to that, here we reported a positive correlation of the above trace elements with microbial parameters. The positive correlation of Cu, Zn, Mg, Fe, and P with microbial parameters might be due to their requirement in microbial activities as these elements are considered essential for microbial metabolism (Liu et al. 2020; Claus 2010; Kaiser and Bollag 1990).

Additionally, microbial enzyme activities exhibited depth dependent phenomena while microbial abundance did not show depth dependent variation. We did not perceive a distinguishable difference in microbial community composition of the upper and lower part of the core based on DGGE profile (Fig. 3.9) This contradictory relationship suggested that microbial abundance and microbial community composition does not have a remarkable influence on microbial enzyme activities but *in-situ* mineral microbes interaction and bioavailability of elements might influence microbial enzyme activities in the CRD core. Overall, a positive correlation of Cu, Zn, Mg, Fe, and P with microbial parameters suggest a participatory role of these elements in microbial mediated biogeochemical cycling and

alternation of these variables could assist future investigation on microbial mediated management of ecosystem functioning of the region. However, further investigations will be needed for understanding in-depth geochemical and microbial characteristics and their correlations in estuarine terrace ecosystem as estuarine ecosystems are highly diverse in their geochemical and microbial characteristics and to confirm the present findings.

### **3.5 Conclusion**

In this study, we illustrated the microbial and physicochemical characteristics together with their correlation in estuarine and fluvial sediment deposits observed at the Chokari (CRD) estuarine terrace (which is ~5 m above the present day high tide level) of the Mahi River (Gujarat, Western India). Higher alkaline phosphatase (P cycle enzyme) and fluorescein diacetate hydrolysis activities were observed as compared to dehydrogenase,  $\beta$ -glucosidase (C cycle enzymes), protease (N cycle enzyme), and arylsulfatase (S cycle enzyme) activities. The enzymatic stoichiometry analysis revealed a P limitation within the estuarine terrace core. Inclusive, detectable microbial enzyme activities throughout the 17 m deep core, functional prediction analysis of microbial community composition, detection of denitrifiers and sulfate-reducing bacteria indicate the role of the Mahi estuarine core in C, N, and S cycling. Microbial diversity analysis carried out by culturable and uncluturable methods (DGGE and metabarcoding) revealed the dominance of bacterial phyla *Actinobacteria*, *Proteobacteria*, *Bacteroidetes*, *Firmicutes*, *Chloroflexi*, and *Acidobacteria* in the Mahi River estuarine core. Correlation analysis between sediment microbial and physicochemical characteristics revealed that total org. C, pH, salinity,  $P_2O_5$ ,  $Fe_2O_3$ , MgO, Cu, and Zn content are the key physicochemical parameters that linked with microbial parameters and could assist in microbial mediated alternation in biogeochemical cycling.